An Affine Continuum Mechanical Model for Cross-Linked F-Actin Networks with Compliant Linker Proteins

Gerhard A. Holzapfel[1]*, Michael J. Unterberger[1] and Ray W. Ogden[2]

[1]*Institute of Biomechanics, Graz University of Technology,*

Kronesgasse 5-I, 8010 Graz, Austria

[2]*School of Mathematics and Statistics, University of Glasgow,*

University Gardens, Glasgow G12 8QW, Scotland, UK

Abstract. Cross-linked actin networks are important building blocks of the cytoskeleton. In order to gain deeper insight into the interpretation of experimental data on actin networks, adequate models are required. In this paper we introduce an affine constitutive network model for cross-linked F-actin networks based on nonlinear continuum mechanics, and specialize it in order to reproduce the experimental behavior of *in vitro* reconstituted model networks. The model is based on the elastic properties of single filaments embedded in an isotropic matrix such that the overall properties of the composite are described by a free-energy function. In particular, we are able to obtain the experimentally determined shear and normal stress responses of cross-linked actin networks typically observed in rheometer tests. In the present study an extensive analysis is performed by applying the proposed model network to a simple shear deformation. The single filament model is then extended by incorporating the compliance of cross-linker proteins and further extended by including viscoelasticity. All that is needed for the finite element implementation is the constitutive model for the filaments, the linkers and the matrix, and the associated elasticity tensor in either the Lagrangian or Eulerian formulation. The model facili-

*To whom correspondence should be addressed. Email address: holzapfel@tugraz.at

tates parameter studies of experimental setups such as micropipette aspiration experiments and we present such studies to illustrate the efficacy of this modeling approach.

Keywords: actin filaments; cross-linker proteins; actin networks; continuum mechanics; finite element analysis

1 Introduction

The cytoskeleton is a network consisting mainly of actin, intermediate filaments and microtubules, which give a cell its shape and its ability for motility and division. The protein actin, in particular, builds a cross-linked isotropic structure underneath the lipid bilayer. *In vitro* reconstituted actin gels, cross-linked with actin-binding proteins, serve as model systems that are characterized by nonlinear stiffening and viscoelastic response [1] in rheological experiments. Furthermore, in rheological torsion experiments they exhibit what is referred to in the biophysics literature as 'negative normal stress'[2], which is exceptional in the sense that the normal stress is opposite to that occurring in polymeric networks of rubber-like materials.

Actin-binding proteins may attach to actin and link two filaments together. They are also referred to as cross-linking proteins or linker proteins or just *linkers*, which is the term we use henceforth. Actin filaments with different linkers are known to form gels, and networks with linkers such as filamin [1, 3, 4], scruin [5, 6] and heavy meromyosin (HMM) in the rigor state [7, 8] are studied extensively. The type of linker strongly influences the mechanical response of the network [4] by changing its morphology. In this sense, according to Tharmann et al. [7], HMM is extraordinary because (i) it creates isotropic networks without any embedded bundles over a large range of linker concentrations; (ii) in actin networks the compliance of

the individual filaments is dominated by their thermal fluctuations, and the compliance of the linkers does not alter this picture; (iii) the mechanics of such networks can be described on the basis of affine deformations.

Continuum mechanical models for cross-linked actin networks seek not only to explain the mechanics of the *in vitro* model systems but also to interpret the results of more complicated experiments in cell mechanics. Many of these models are based on the microstructure of the network and adopt the idea of integrating the single filament response into a network [9]. For example, an algorithmic treatment for affine and non-affine networks, the micro-sphere model, was introduced by Miehe et al. [10] and the affine network model was adopted for modeling the mechanics of collagen in arteries [11, 12]. Applications of the filament-to-network approach to the elasticity of actin networks have also been proposed [13, 14]. In particular, Unterberger et al. [14] use a non-affinity parameter that is not intuitive, while a recently introduced model [15] facilitates the understanding of non-affinity but it turns out to be very expensive in terms of computational cost and is therefore not very practical.

Based on a continuum mechanical framework, we show that an affine full network model is capable of capturing not only the shear stress but also the normal stress behavior of semi-flexible biopolymer networks. We use scaling arguments from the literature to relate material parameters to protein concentrations of samples in bulk rheology. Furthermore, we include a contribution from compliant linkers in the continuum model which has the effect of softening actin gels. The model is also enhanced by including a viscoelastic contribution. The calibration of the proposed model is performed with data from rheological torsion experiments. The model can be used to interpret experiments with more complicated geometries and boundary

conditions such as atomic force microscopy or micropipette aspiration, and can also be used for parameter studies in virtual experiments.

We introduce a continuum mechanical framework and an incompressible elastic network model in Section 2. It is then applied to simple shear deformation, showing in particular that it predicts the correct normal stress response. The elastic model is next extended to include the effects of compliant linkers. Since this is the first application of a continuum mechanics based inclusion of compliant linkers we assume for simplicity that the linkers are anchored to the actin filaments and that there are no mechanical interactions between the filaments. In Section 3 a compressible version of the model is formulated in order to facilitate a finite element implementation. In particular, it is based on the multiplicative split of the deformation gradient into volumetric and isochoric parts, and the stress and elasticity tensors are also provided. This is also extended to include viscoelastic effects. Some aspects of the numerical treatment of the proposed model in a finite element program and a representative numerical example that includes cross-linking and viscoelastic effects are provided in Section 4. We finalize the study with a summary and concluding remarks.

2 Analysis of Incompressible Elastic Filamentous Networks

Consider a soft elastic continuum which is deformed so that the deformation gradient is $\mathbf{F}$ and the right Cauchy–Green tensor is $\mathbf{C} = \mathbf{F}^{\mathrm{T}}\mathbf{F}$. Here we consider the continuum as incompressible so that the volume ratio $J = \det\mathbf{F} = 1$. Suppose that a distribution of filaments is embedded in this material, which we refer to as the matrix, and the filaments deform affinely with the matrix. Suppose that a typical filament has orientation $\mathbf{M}$ in the reference configuration which maps to

m in the current configuration as

$$\mathbf{m} = \mathbf{FM}. \tag{1}$$

The stretch $\lambda\,(>0)$ in the direction **M**, i.e. along the mean end-to-end distance of the filament, is defined by

$$\lambda^2 = \mathbf{M}\cdot\mathbf{CM} = \mathbf{m}\cdot\mathbf{m}. \tag{2}$$

We emphasize that **m** is aligned with the corresponding mean end-to-end distance of the filament in the deformed configuration, as will be discussed in Section 2.4. Let $\rho(\mathbf{M})$ be the relative angular density of filaments so that

$$\frac{1}{4\pi}\int_\Omega \rho(\mathbf{M})\,\mathrm{d}\Omega = 1, \tag{3}$$

where Ω is the unit sphere. The free energy of a single filament is $w(\lambda)$ so that by assuming that all filaments have the same properties, i.e. the same form of $w(\lambda)$, the free energy over all orientations is

$$n\int_\Omega \rho(\mathbf{M})w(\lambda)\mathrm{d}\Omega, \tag{4}$$

where n is the numbers of filaments per unit reference volume. If there are different types of filaments with energies $w_k(\lambda)$, number of filaments n_k, and densities $\rho_k(\mathbf{M})$, $k = 1, 2, 3\ldots$, then (4) is replaced by

$$\sum_k n_k\int_\Omega \rho_k(\mathbf{M})w_k(\lambda)\mathrm{d}\Omega, \tag{5}$$

and (3) by

$$\sum_k \frac{1}{4\pi}\int_\Omega \rho_k(\mathbf{M})\,\mathrm{d}\Omega = 1. \tag{6}$$

Now for simplicity we consider only one type of filament so that (4) serves as the basis for the analysis. Suppose the volume fraction of filaments is φ and that of the isotropic matrix is

$1-\varphi$. For the matrix and the filaments the free-energy function Ψ per unit reference volume is then

$$\Psi(\mathbf{C},\mathbf{M}) = n\int_{\Omega}\rho(\mathbf{M})w(\lambda)\mathrm{d}\Omega + (1-\varphi)\Psi_{\mathrm{mat}}(\mathbf{C}), \tag{7}$$

where Ψ_{mat} is the free energy of the matrix material per unit reference volume. The volume fraction of the filaments is $\varphi = nLS_0$, where L is the contour length of a single filament and S_0 is its reference cross-sectional area assuming all filaments have the same contour length and cross-sectional area. The volume fraction φ for, for example, F-actin gel can be as low as 0.001% [16]. Note that in general w depends on the material constants which themselves depend on the concentration and compliance of linkers (which for F-actin are referred to as actin-binding proteins), and these are included implicitly in the form of w. Factors which need to be taken into consideration are the lengths of the filaments between the linkers, the concentration of actin and the concentration of linkers. These will be made explicit in Sections 2.4 and 2.5. In terms of the length scale we suggest to use the model within the micron-scale domain, say 10 times the filament length. For example, [17] have used a simulation domain of $5\,\mu$m only, which is perfectly acceptable for a continuum mechanics approach.

From the free-energy function we calculate the mechanical stress in the material using the standard continuum mechanical framework. In particular, the Cauchy stress tensor $\boldsymbol{\sigma}$ is defined by

$$\boldsymbol{\sigma} = 2\mathbf{F}\frac{\partial\Psi}{\partial\mathbf{C}}\mathbf{F}^{\mathrm{T}} - p\mathbf{I}, \tag{8}$$

where p is a Lagrange multiplier associated with the incompressibility constraint, and can be identified as a hydrostatic pressure, and $\mathbf{I}$ is the second-order identity tensor. Hence, with the

free-energy function (7) we obtain

$$\boldsymbol{\sigma} = n \int_{\Omega} \rho(\mathbf{M}) \lambda^{-1} w'(\lambda) \mathbf{m} \otimes \mathbf{m} \, \mathrm{d}\Omega + 2(1-\varphi) \mathbf{F} \frac{\partial \Psi_{\mathrm{mat}}}{\partial \mathbf{C}} \mathbf{F}^{\mathrm{T}} - p\mathbf{I}, \tag{9}$$

where the prime is used as a convenient shorthand notation, i.e. $(\bullet)' = \mathrm{d}(\bullet)/\mathrm{d}\lambda$. In the derivation of (9) we have used the property

$$\frac{\partial(\lambda^2)}{\partial \mathbf{C}} = \mathbf{M} \otimes \mathbf{M} \tag{10}$$

obtained from (2) together with (1).

2.1 Application to Simple Shear

Experiments on networks using rheometers produce torsion, which is commonly approximated as simple shear (see, for example, [18]). We study this mode of deformation because the behavior in shear has been highlighted as unusual in the literature [2] and it is the only mode for which experimental results have been reported.

For simple shear, in the (X_1, X_2) plane, the matrix of $\mathbf{F}$ is given by

$$[\mathbf{F}] = \begin{bmatrix} 1 & \gamma & 0 \\ 0 & 1 & 0 \\ 0 & 0 & 1 \end{bmatrix}, \tag{11}$$

where γ is the amount of shear, which, without loss of generality, we take to be positive. In terms of spherical polar angles Θ and Φ the filament direction $\mathbf{M}$ has Cartesian components

$$[\mathbf{M}] = [\sin\Theta\cos\Phi, \sin\Theta\sin\Phi, \cos\Theta]^{\mathrm{T}}, \tag{12}$$

where $\Theta \in [0, \pi]$ and $\Phi \in [-\pi, \pi]$. Then the corresponding vector in the deformed configuration

has components

$$[\mathbf{m}] = [\mathbf{F}][\mathbf{M}] = \begin{bmatrix} \sin\Theta(\cos\Phi + \gamma\sin\Phi) \\ \sin\Theta\sin\Phi \\ \cos\Theta \end{bmatrix}, \tag{13}$$

and hence

$$\lambda^2 = \mathbf{m}\cdot\mathbf{m} = 1 + \sin^2\Theta(\gamma\sin 2\Phi + \gamma^2\sin^2\Phi). \tag{14}$$

If the filaments are equally distributed in all directions then $\rho = 1$ and the material is isotropic. Henceforth we restrict the attention to the case $\rho = 1$. Then, from (9) we obtain

$$\boldsymbol{\sigma} = n\int_\Omega \lambda^{-1}w'(\lambda)\mathbf{m}\otimes\mathbf{m}\sin\Theta\mathrm{d}\Theta\mathrm{d}\Phi + \boldsymbol{\sigma}_{\mathrm{mat}}, \quad \boldsymbol{\sigma}_{\mathrm{mat}} = 2(1-\varphi)\mathbf{F}\frac{\partial\Psi_{\mathrm{mat}}}{\partial\mathbf{C}}\mathbf{F}^{\mathrm{T}} - p\mathbf{I}, \tag{15}$$

where $\boldsymbol{\sigma}_{\mathrm{mat}}$ is the part of the stress due to the matrix.

By using $(15)_1$ and (13) the components of stress are then given by

$$\sigma_{11} = n\int_\Omega \lambda^{-1}w'(\lambda)(\cos\Phi + \gamma\sin\Phi)^2\sin^3\Theta\mathrm{d}\Theta\mathrm{d}\Phi + \sigma_{\mathrm{mat}\,11}, \tag{16}$$

$$\sigma_{22} = n\int_\Omega \lambda^{-1}w'(\lambda)\sin^2\Phi\sin^3\Theta\mathrm{d}\Theta\mathrm{d}\Phi + \sigma_{\mathrm{mat}\,22}, \tag{17}$$

$$\sigma_{33} = n\int_\Omega \lambda^{-1}w'(\lambda)\cos^2\Theta\sin\Theta\mathrm{d}\Theta\mathrm{d}\Phi + \sigma_{\mathrm{mat}\,33}, \quad \sigma_{13} = \sigma_{23} = 0, \tag{18}$$

$$\sigma_{12} = n\int_\Omega \lambda^{-1}w'(\lambda)\sin\Phi(\cos\Phi + \gamma\sin\Phi)\sin^3\Theta\mathrm{d}\Theta\mathrm{d}\Phi + \sigma_{\mathrm{mat}\,12}. \tag{19}$$

We recall that for an isotropic material the universal relation [19, Eq. (4.4.15)]

$$\sigma_{\mathrm{mat}\,11} - \sigma_{\mathrm{mat}\,22} - \gamma\sigma_{\mathrm{mat}\,12} = 0 \tag{20}$$

holds. It can then be shown that this relation also holds for the total stress used here, i.e.

$$\sigma_{11} - \sigma_{22} - \gamma\sigma_{12} = n\int_\Omega \lambda^{-1}w'(\lambda)(\cos 2\Phi + \gamma\sin\Phi\cos\Phi)\sin^3\Theta\mathrm{d}\Theta\mathrm{d}\Phi = 0. \tag{21}$$

This follows since, for fixed values of Θ and γ, we obtain from $(14)_2$

$$\lambda \mathrm{d}\lambda = \gamma \sin^2\Theta(\cos 2\Phi + \gamma \sin\Phi\cos\Phi)\mathrm{d}\Phi. \tag{22}$$

If we change the variables Φ to λ in $(21)_2$ then we obtain

$$\frac{n}{\gamma}\int_{\Theta}\sin\Theta\int_{\lambda} w'(\lambda)\mathrm{d}\lambda\mathrm{d}\Theta. \tag{23}$$

The relevant ranges of values of Θ and Φ are $0 \to \pi$ and $0 \to \Phi_0$, respectively. But if we regard λ as a function of Θ and Φ and write $\lambda(\Theta,\Phi)$ then $\lambda(\Theta,0) = \lambda(\Theta,\Phi_0) = 1$ and the λ-integral in (23) vanishes. Thus, the universal relation (21) holds.

In general we take $w'(\lambda) > 0$ for $\lambda > 1$, i.e. tension corresponds to extension. We also assume that the filament does not support compression and hence set $w'(\lambda) = 0$ for $\lambda \leq 1$ and we therefore exclude any contribution of $w'(\lambda)$ from the integration for the angles for which $\lambda \leq 1$. The values of Φ for which $\lambda = 1$ are 0, Φ_0 and $\Phi_0 + \pi$, where Φ_0 is given by $\tan\Phi_0 = -2/\gamma$. The value of λ is plotted in the color-coded Fig. 1 in the (X_1,X_2)-plane. We obtain values of $\lambda \geq 1$ in the two regions of Φ defined by $[-\pi,\Phi_0]\cup[0,\Phi_0+\pi]$. The boundaries of the integration domain are indicated by black lines in the figure. For the angle Θ, the integration domain is $[0,\pi]$. Note that the orientation of the Lagrangian principal axes in the (X_1,X_2)-plane (with $\Theta = 0$) is given by $\tan 2\Phi = -2/\gamma$, [19, Eq. (2.2.59)]. With reference to Fig. 1 it can be seen that the direction of maximum stretch is given by $\Phi = \Phi_{\mathrm{r}}$, where

$$\Phi_{\mathrm{r}} = \frac{\Phi_0 + \pi}{2} \tag{24}$$

in the reference configuration. Hence, $\tan 2\Phi_{\mathrm{r}} = \tan\Phi_0 = -2/\gamma$, and therefore the direction of maximum stretch is a Lagrangian principal axis.

2.2 Integration Limits for Arbitrary Deformations

We now take a closer look at the integration domain using the spectral decomposition of the right Cauchy–Green tensor $\mathbf{C} = \lambda_a^2 \mathbf{N}_a \otimes \mathbf{N}_a$, where $a = 1, 2, 3$, λ_a are the principal stretches (positive square roots of the eigenvalues of $\mathbf{C}$) and the unit vectors $\mathbf{N}_a$ are the principal referential directions (eigenvectors of $\mathbf{C}$). The values of the principal stretches can be ordered so that $\lambda_1 \geq \lambda_2 \geq \lambda_3$. Then, we choose the coordinate system so that the principal direction associated with the first principal stretch λ_1 is oriented with $\Theta = \pi/2$ and $\Phi = 0$, the second principal stretch λ_2 corresponds to the principal direction for which $\Theta = \pi/2$ and $\Phi = \pi/2$, while λ_3 is associated with $\Theta = 0$. Then, for incompressible materials ($\lambda_1\lambda_2\lambda_3 = 1$)

$$\lambda^2 = \lambda_1^2 \sin^2\Theta \cos^2\Phi + \lambda_2^2 \sin^2\Theta \sin^2\Phi + \frac{1}{\lambda_1^2\lambda_2^2} \cos^2\Theta. \tag{25}$$

Figure 2 illustrates the topology of the squared stretch in the (Θ,Φ)-plane for the selected principal stretches $[\lambda_1, \lambda_2, \lambda_3] = [1.50, 1.026, 0.65]$. The integration domain contributing to the Cauchy stress tensor (9) is the region where λ^2 is above the plane defined by $\lambda^2 = 1$.

We also distinguish several cases with different integration area shapes in terms of the principal stretches, as illustrated in Fig. 3. Therein, the grey area indicates the relevant integration area in the (Φ,Θ)-plane. The specific deformation of Fig. 2 is represented in Fig. 3(a) together with three deformation modes (b)–(d), which correspond to equibiaxial extension or unconfined compression, pure shear or simple shear in the $(1, 3)$-plane and uniaxial extension, respectively. In each case the area is π-periodic in Φ. This means that when the unit sphere of integration is divided in two hemispheres, λ possesses rotational symmetry between the hemispheres. This important property may be exploited when applying a numerical scheme for evaluating the integral in (9) in the case of isotropy, as is done in Section 4.

2.3 Specialization of the Material Model

Consider now an isotropic matrix material for which the free energy $\Psi_{\rm mat}$ is a function of the invariants I_1 and I_2 of the left Cauchy–Green tensor $\mathbf{b} = \mathbf{F}\mathbf{F}^{\rm T}$, where $I_1 = \operatorname{tr}\mathbf{b}$ and $I_2 = \operatorname{tr}(\mathbf{b}^{-1})$. By recalling $(15)_2$, the Cauchy stress tensor is then given by (see, e.g., [19, 20])

$$\boldsymbol{\sigma}_{\rm mat} = 2(1-\varphi)[\psi_1\mathbf{b} + \psi_2(I_1\mathbf{b} - \mathbf{b}^2)] - p\mathbf{I}, \tag{26}$$

where $\psi_i = \partial\Psi_{\rm mat}/\partial I_i$, $i = 1, 2$. For simple shear

$$[\mathbf{b}] = \begin{bmatrix} 1+\gamma^2 & \gamma & 0 \\ \gamma & 1 & 0 \\ 0 & 0 & 1 \end{bmatrix}, \tag{27}$$

and hence

$$\sigma_{\rm mat\,22} - \sigma_{\rm mat\,33} = -2\psi_2\gamma^2(1-\varphi). \tag{28}$$

Without loss of generality we may take $\sigma_{33} = 0$ because of the incompressibility constraint (p is arbitrary). Then from (18)

$$\sigma_{\rm mat\,33} = -n\int \lambda^{-1}w'(\lambda)\cos^2\Theta\sin\Theta{\rm d}\Theta{\rm d}\Phi \tag{29}$$

and (17) gives

$$\sigma_{22} = n\int_\Omega \lambda^{-1}w'(\lambda)\left(\sin^2\Phi\sin^3\Theta - \cos^2\Theta\sin\Theta\right){\rm d}\Theta{\rm d}\Phi - 2\psi_2\gamma^2(1-\varphi). \tag{30}$$

For material models such as the (incompressible isotropic) Mooney–Rivlin model below, ψ_2 is positive and thus the second term is *negative*. Similarly,

$$\sigma_{12} = n\int_\Omega \lambda^{-1}w'(\lambda)\sin\Phi(\cos\Phi + \gamma\sin\Phi)\sin^3\Theta{\rm d}\Theta{\rm d}\Phi + 2(1-\varphi)(\psi_1+\psi_2)\gamma, \tag{31}$$

wherein the second term is *positive* since $2(\psi_1 + \psi_2)$ equals the shear modulus μ of the matrix when evaluated in the reference configuration, and is therefore assumed to be positive in the deformed configuration.

For the Mooney–Rivlin model $\Psi_{\rm mat}$ is given by

$$\Psi_{\rm mat} = c_1(I_1 - 3) + c_2(I_2 - 3), \tag{32}$$

where c_1, c_2 are positive material constants. Then, from (28) and (29), we obtain

$$\sigma_{\rm mat\,22} = -2c_2\gamma^2(1-\varphi) - n\int_\Omega \lambda^{-1}w'(\lambda)\cos^2\Theta\sin\Theta\,\mathrm{d}\Theta\,\mathrm{d}\Phi, \quad \sigma_{\rm mat\,12} = (1-\varphi)\mu\gamma, \tag{33}$$

with $\mu = 2(c_1 + c_2)$.

In the integrands of (16)–(19) we need the term $\lambda^{-1}w'$. When λ is close to one (γ is small) the integrals can be formed explicitly because, when expanded to the second order in γ, we obtain, with the help of (14),

$$\begin{aligned}\lambda^{-1}w'(\lambda) \sim\ & w''(1)[\gamma\sin^2\Theta\sin\Phi\cos\Phi + \frac{1}{2}\gamma^2\sin^2\Theta\sin^2\Phi - \gamma^2\sin^4\Theta\sin^2\Phi\cos^2\Phi] \\ & + \frac{1}{2}w'''(1)\gamma^2\sin^4\Theta\sin^2\Phi\cos^2\Phi,\end{aligned} \tag{34}$$

which is correct to the second order in γ. By using standard trigonometric integrals with the integration domain $[-\pi/2, \pi/2]$ depicted in Fig. 3(c), then (30), in particular, yields

$$\sigma_{22} \sim \underbrace{nw''(1)\left(\frac{4}{15}\gamma + \frac{2\pi}{21}\gamma^2\right) + nw'''(1)\frac{2\pi}{15}\gamma^2}_{\flat}\ \underbrace{-2c_2\gamma^2}_{\sharp}(1-\varphi), \tag{35}$$

where the term $\flat$ is > 0 under our assumptions, and the term $\sharp$ is < 0 with the Mooney–Rivlin material parameter $c_2 > 0$.

For the neo-Hookean material $c_2 = 0$ and σ_{22} is positive. In this case the network model requires a positive normal stress to maintain the simple shear. Hence, the network model generates a positive normal stress (which is called a 'negative normal stress' in the biophysics

literature [2]). Note that not all forms of w would predict a positive normal stress. If the sample height were not constrained then the material would become thinner in the X_2-direction.

2.4 Application to a Specific Filament Free-Energy Function $w(\lambda)$

First we consider an inextensible single filament with the contour length L, mean end-to-end distance r_0 in the unloaded state and r in the loaded state. Then we define the stretch λ as r/r_0. When the filament is embedded in the continuum, λ is also given by $(14)_2$ for a simple shear deformation. The force f required to extend the filament can be written as $f = \mathrm{d}w/\mathrm{d}r = w'/r_0$, where $w(\lambda)$ is the free energy of the filament. For the considered inextensible filament we also make use of the bending stiffness B_0 which is given as $k_{\mathrm{B}}TL_{\mathrm{p}}$, where $k_{\mathrm{B}} = 1.38 \cdot 10^{-23}$ Nm/K is the Boltzmann constant, T is the ambient temperature and L_{p} is the persistence length. We now take w to be of the form defined in [21] for which $w'(\lambda)$ is [14, 21, 22]

$$w'(\lambda) = \frac{\pi^2 r_0 B_0}{L^2}\left[\left(\frac{a-1}{a-\lambda}\right)^{\delta} - 1\right], \tag{36}$$

where $a = L/r_0$ and $\delta \geq 1$ is a constant. Then from (30) and (31) with (36) we obtain the total normal and shear stresses as

$$\sigma_{22} = n\frac{\pi^2 B_0}{aL}\int_{\Omega} \lambda^{-1}\left[\left(\frac{a-1}{a-\lambda}\right)^{\delta} - 1\right]\left(\sin^2\Phi\sin^3\Theta - \cos^2\Theta\sin\Theta\right)\mathrm{d}\Theta\mathrm{d}\Phi$$
$$-2c_2\gamma^2(1-\varphi), \tag{37}$$

$$\sigma_{12} = n\frac{\pi^2 B_0}{aL}\int_{\Omega} \lambda^{-1}\left[\left(\frac{a-1}{a-\lambda}\right)^{\delta} - 1\right]\sin\Phi(\cos\Phi + \gamma\sin\Phi)\sin^3\Theta\mathrm{d}\Theta\mathrm{d}\Phi$$
$$+\mu\gamma(1-\varphi). \tag{38}$$

Finally, if required, the component σ_{11} can be obtained from the universal relation (21). The properties of the Mooney–Rivlin material are well known, and hence we are only interested in

evaluating the contribution to the stresses of the filaments. For this purpose we only need to consider the integrals in (37) and (38).

Since the filament model is inextensible, the filament locks ($f \to \infty$) when $r \to L$. Then locking of the bulk material appears when $\lambda \to a$ for the filaments in the direction of the maximum principal stretch at the critical amount of shear γ_{crit}. This situation is reached when

$$1 + \gamma_{\text{crit}} \sin 2\Phi_{\text{r}} + \gamma_{\text{crit}}^2 \sin^2 \Phi_{\text{r}} = a^2 \tag{39}$$

holds, where we have used (14) with $\Theta = \pi/2$. Relation (39) can also be written as

$$\tan \Phi_{\text{r}} = a, \qquad \gamma_{\text{crit}} = a - a^{-1}, \tag{40}$$

where (24) has been used. As an example, for $a = 1.2$ we obtain $\Phi_{\text{r}} = 50.2^\circ$ and $\gamma_{\text{crit}} = 0.36$.

The material parameters r_0 and n can be related to experimental inputs. In bulk rheology samples are prepared with a defined concentration c_{actin} of actin monomers and a concentration c_{ABP} of actin-binding proteins (ABPs). Based on considerations of MacKintosh et al. [23] the scaling of the distance between two linkers, which we now denote by r_0, was derived for rigor HMM/actin networks by Tharmann et al. [7]. In particular, with $c_{\text{actin}} = 9.5\,\mu\text{M}$ ($1\,\text{M} = 1\,\text{mol/l}$) and a constant L_{p} they fitted data to arrive at (see the inset of Fig. 3(b) in [7])

$$r_0 = 1.6\, c_{\text{ABP}}^{-2/5}, \tag{41}$$

where r_0 is in μm and c_{ABP} is given in μM.

The relationship between n and c_{actin} with a given contour length L was derived earlier [14] (see also [13]) to be

$$n = \frac{c_{\text{actin}} N_{\text{A}} M_{\text{actin}}}{L \rho_{\text{actin}}}, \tag{42}$$

Table 1: Material parameters derived for three linker concentrations from (41), $L = 1.2r_0$ and (42).

$c_{\mathrm{ABP}}(\mu\mathrm{M})$	$r_0\ (\mu\mathrm{m})$	$L\ (\mu\mathrm{m})$	$n\ (\mu\mathrm{m}^{-3})$
0.95	1.63	1.96	7.66
0.475	2.15	2.58	5.82
0.238	2.83	3.40	4.42

where $N_{\mathrm{A}} = 6.022 \cdot 10^{23}\,\mathrm{mol}^{-1}$ is the Avogadro constant, $M_{\mathrm{actin}} = 42\,\mathrm{kDa}$ is the molecular mass of each actin monomer and $\rho_{\mathrm{actin}} = 16\,\mathrm{MDa}/\mu\mathrm{m}$ is the actin density.

Plots of σ_{22} and σ_{12} versus γ without a matrix ($c_1 = c_2 = 0$) are shown in Fig. 4(a) and (b), respectively. In addition, in Fig. 4(c) is plotted the shear modulus $\partial\sigma_{12}/\partial\gamma$, which is a widely used measure of the network stiffness in the biophysics literature. In each case three different values of c_{ABP} are used with an actin concentration of $c_{\mathrm{actin}} = 9.5\,\mu\mathrm{M}$ and an ambient temperature $T = 294\,\mathrm{K}$, a persistence length of $L_{\mathrm{p}} = 16\,\mu\mathrm{m}$ [24] and $\delta = 2$. We assume that the contour length of the filament is 20% longer than its end-to-end distance, i.e. $a = L/r_0 = 1.2$. The material parameters r_0, L and n are derived from (41), the definition of a and (42), respectively. In Table 1 we summarize the values of the three concentrations used $c_{\mathrm{ABP}} = 0.95$, 0.475 and $0.238\,\mu\mathrm{M}$, i.e. $1/10$, $1/20$, $1/40$, of the actin concentration.

The curves in Fig. 4 reproduce the overall behavior of actin gels cross-linked with HMM very well [7, 14] except for values of γ very close to the asymptote defined by (40). The appearance of the asymptote is associated with the assumption of inextensibility used here. A particular characteristic is the soft initial response followed by the pronounced nonlinear

stiffening for both stress components. The shear and normal stresses are of the same order of magnitude, as reported previously [2, 14]. The shear modulus $\partial\sigma_{12}/\partial\gamma$ is relatively constant for small γ and approaches infinity when as the asymptote is approached. As already mentioned the asymptote arises because of the choice of the inextensible filament model, and this leads to unphysical behavior of the model for strains $\gamma > 0.25$. The equation (9), however, allows one to use any extensible filament model instead; see, e.g., Appendix A and the references therein. This would eliminate the infinite stiffness at the critical amount of shear γ_{crit} and would lead to a shear modulus at high values of γ comparable to that in [7].

2.5 A Model Incorporating Compliant Linkers

Now consider a compound filament, as depicted in Fig. 5(a), and its inclusion within a microsphere in Fig. 5(b), which is utilized for the finite element implementation of the model that will be introduced in Section 3. It consists of an actin filament and a flexible linker protein. We assume that the linker can only carry loads in its axial direction. In the reference configuration no force is applied and the actin filament and linker have end-to-end distances $r_{0,\text{f}}$ and $r_{0,\text{c}}$, respectively, so that the total end-to-end distance is $r_0 = r_{0,\text{f}} + r_{0,\text{c}}$. Upon deformation the filament and linker end-to-end distances change to r_f and r_c and the total end-to-end distance to

$$r = r_\text{f} + r_\text{c}. \tag{43}$$

We also define the ratios of the end-to-end distances as

$$\lambda_\text{f} = r_\text{f}/r_{0,\text{f}}, \qquad \lambda_\text{c} = r_\text{c}/r_{0,\text{c}} \tag{44}$$

and we recall that $r = \lambda r_0$. Combining these definitions we obtain

$$\lambda r_0 = \lambda_\text{f} r_{0,\text{f}} + \lambda_\text{c} r_{0,\text{c}}. \tag{45}$$

The free energy in a compound filament is $w(\lambda) = w_{\rm f}(\lambda_{\rm f}) + w_{\rm c}(\lambda_{\rm c})$, where $w_{\rm f}$ and $w_{\rm c}$ are the free energies of the filament and the linker, respectively. This is related to the force acting on the filament compound. Based on the formula (36) we now define the force $f_{\rm f}$ acting on the filaments by

$$f_{\rm f}(\lambda_{\rm f}) = \frac{\pi^2 B_0}{L^2}\left[\left(\frac{a-1}{a-\lambda_{\rm f}}\right)^{\delta} - 1\right], \tag{46}$$

where we now consider only $\lambda_{\rm f}$, as defined in $(44)_1$. Because knowledge of the compliance of linkers is limited we consider nonlinear linkers which have a stiffness related to that of the actin filaments. Note, however, that the force $f_{\rm c}$ acting on the linker must be equal to that acting on the filament, i.e. $f_{\rm f}$, and we therefore drop the subscript and write $f = f_{\rm c} = f_{\rm f}$; see the free body diagram in Fig. 5(a). We decompose the elongation of the compound $\Delta r = r - r_0$ into the elongation of the filament $\Delta r_{\rm f} = r_{\rm f} - r_{0,\rm f}$ and the elongation of the linker $\Delta r_{\rm c} = r_{\rm c} - r_{0,\rm c}$ so that $\Delta r = \Delta r_{\rm f} + \Delta r_{\rm c}$. Assume now that the equal forces in the linker and the filament result in the relationship

$$\Delta r_{\rm f} = \eta \Delta r, \tag{47}$$

where $\eta \in (0, 1]$ is a material parameter, which could be a function of Δr, that modulates the linker stiffness. Henceforth we refer to η as a *relative linker stiffness*. One endpoint of the interval corresponds to the case of a rigid linker with $\eta = 1$. The absence of the linker corresponds to the case $\eta = 0$ for which in (47) we consider $\eta \Delta r_{\rm c}$ as tending to a finite limit as η tends to zero. Using $(44)_1$ and $r = \lambda r_0$, we obtain

$$\lambda_{\rm f} = \eta \frac{r_0}{r_{0,\rm f}}(\lambda - 1) + 1, \tag{48}$$

and $\lambda_{\rm c}$ may be obtained from (45).

We now use the above considerations in the network setting. The force $f = f_{\mathrm{f}}$ is calculated from (46) as a function of λ by using (48) and is also given by the derivative of the free energy with respect to λ, i.e. $w'(\lambda) = f r_0$, which can then be used in (9) to determine the Cauchy stress tensor.

We use the parameter set for $c_{\mathrm{ABP}} = 0.95\,\mu\mathrm{M}$ from Table 1 and we note that the end-to-end distance r_0 therein is replaced by $r_{0,\mathrm{f}}$ in this section. Normal stress σ_{22}, shear stress σ_{12} and shear modulus $\partial\sigma_{12}/\partial\gamma$ are plotted in Fig. 6 for $\eta = 1, 2/3$ and $1/3$. Note that the dash-dotted curves for $\eta = 1$, coincide with the corresponding curves in Fig. 4. The characteristics of the curves are similar for all η. The less stiff the linker is compared to the filament, i.e. the smaller η is, the softer is the overall response of the bulk material. The asymptote of the curves shifts to higher amounts of shear as η is decreased. The asymptote can be determined by substituting (48) into (46) and then noting that the resulting denominator vanishes for $\lambda^2 = [r_{0,\mathrm{f}}(a-1)/(\eta r_0) + 1]^2$, which is then used to replace a^2 in (39) in order to calculate γ_{crit}. With the numbers used we obtain $\gamma_{\mathrm{crit}} = 0.53$ and 0.98 for $\eta = 2/3$ and $1/3$, respectively.

It is interesting to compare the results from the model with experimental data, specifically for cross-linked actin networks with different types of linkers but equal concentrations $c_{\mathrm{actin}} = 9.5\,\mu\mathrm{M}$ and $c_{\mathrm{ABP}} = 0.95\,\mu\mathrm{M}$. The values in the curves for the linker with $\eta = 1$ in Fig. 6 are of the same order as the data presented for actin networks cross-linked with HMM in its rigor form [14]. On the other hand the shear modulus data with filamin as the linker [25] are well reflected by the curve in Fig. 6(c) for $\eta = 1/3$. Neglecting other arguments, e.g., interaction of filaments, rotational stiffness of linkers etc., these observations suggest that the stiffness of linkers is a key property of cross-linked actin networks.

A very recent paper [26] models the cross-links as worm-like chain springs and each filament with 100 equal-sized Timoshenko beam elements with the assumption of linear elasticity and without considering the properties of a matrix. The model predicts that flexible cross-links give rise to positive normal stress during small strains but as the shear strains increase the normal stress becomes negative (here we are using the biophysics terminology).

3 Towards Finite Element Implementation

In order to use the model developed in Section 2 in the analysis of realistic boundary-value problems associated with experimental tests it is appropriate to implement it in a finite element program. We therefore introduce here a compressible formulation of the model with a penalty term that is used to accommodate the incompressibility condition numerically. Hence, we base the formulation on a multiplicative split of the deformation gradient and derive the stress and the related elasticity tensors that are required in a finite element environment.

We make use of the volume ratio $J = \det\mathbf{F} > 0$ to define the volume preserving (isochoric) part of $\mathbf{F}$ as $\overline{\mathbf{F}}$ and its volumetric part as $J^{1/3}\mathbf{I}$, where $\det\overline{\mathbf{F}} = 1$. We also define the isochoric right Cauchy–Green tensor $\overline{\mathbf{C}} = \overline{\mathbf{F}}^{\mathrm{T}}\overline{\mathbf{F}}$ so that

$$\mathbf{F} = J^{1/3}\overline{\mathbf{F}}, \qquad \mathbf{C} = J^{2/3}\overline{\mathbf{C}}. \tag{49}$$

With reference to (1) and use of $(49)_1$ we define $\overline{\mathbf{m}}$ as

$$\overline{\mathbf{m}} = \overline{\mathbf{F}}\mathbf{M} = J^{-1/3}\mathbf{m}, \tag{50}$$

and the modified stretch $\bar{\lambda} = J^{-1/3}\lambda$ by

$$\bar{\lambda}^2 = \mathbf{M}\cdot\overline{\mathbf{C}}\mathbf{M} = \overline{\mathbf{m}}\cdot\overline{\mathbf{m}}. \tag{51}$$

The free energy of a single filament is here denoted by $w_{\text{iso}}(\bar{\lambda})$, which replaces $w(\lambda)$ in (7). The free-energy function (for the matrix and the filaments) Ψ_{iso} per unit reference volume, which is the counterpart of (7), is then

$$\Psi_{\text{iso}}(\overline{\mathbf{C}}, \mathbf{M}) = n \int_{\Omega} \rho(\mathbf{M}) w_{\text{iso}}(\bar{\lambda}) \, \mathrm{d}\Omega + (1 - \varphi) \Psi_{\text{iso}}^{\text{mat}}(\overline{\mathbf{C}}), \tag{52}$$

where $\Psi_{\text{iso}}^{\text{mat}}$ is the isochoric free energy of the matrix material per unit reference volume. In addition to (52) there is a given scalar-valued function Ψ_{vol} of J, describing the volumetric (dilatational) elastic response of the material, which contributes to the total free energy Ψ, which is then $\Psi = \Psi_{\text{vol}}(J) + \Psi_{\text{iso}}(\overline{\mathbf{C}}, \mathbf{M})$. For numerical purposes we use here

$$\Psi_{\text{vol}}(J) = \kappa \mathcal{G}, \qquad \mathcal{G} = \frac{1}{4}(J^2 - 1 - 2 \ln J), \tag{53}$$

where κ is a (positive) penalty parameter and $\mathcal{G}$ serves only as a penalty function introduced to accommodate incompressibility. The penalty method for incompressibility is the basis for the numerical approach; see also Section 8.3 in [27].

However, transient behavior is always present in biopolymer networks, and we shall consider this phenomenon by means of an additive extension of the elasticity model using viscous terms. A method for doing this within the framework of nonlinear continuum mechanics at finite strains was introduced by Simo [28] (see also Holzapfel [20, 29]), and it was recently used for modeling cross-linked actin networks [30]. We shall display only the key equations and refer for further details of this to the relevant papers above.

While the modified right Cauchy–Green tensor $\overline{\mathbf{C}}$ characterizes the isochoric part of the elastic deformation, we keep track of the viscous contributions using m strain-like internal variables $\boldsymbol{\Gamma}_{\upsilon}$, $\upsilon = 1, \ldots, m$, akin to $\overline{\mathbf{C}}$. The non-equilibrium response is then described by the

configurational free energies Υ_υ, and the free-energy function Ψ is split additively, in the form

$$\Psi = \Psi_{\text{vol}}(J) + \Psi_{\text{iso}}(\overline{\mathbf{C}}, \mathbf{M}) + \sum_{\upsilon=1}^{m} \Upsilon_\upsilon(\overline{\mathbf{C}}, \boldsymbol{\Gamma}_\upsilon). \tag{54}$$

3.1 Second Piola–Kirchhoff Stress Tensor

The split in (54) results in an analogous split of the total second Piola–Kirchhoff stress tensor $\mathbf{S} = 2\partial\Psi/\partial\mathbf{C}$, i.e.

$$\mathbf{S} = \mathbf{S}_{\text{vol}}(J) + \mathbf{S}_{\text{iso}}(\overline{\mathbf{C}}, \mathbf{M}) + \sum_{\upsilon=1}^{m} \mathbf{Q}_\upsilon(\overline{\mathbf{C}}, \boldsymbol{\Gamma}_\upsilon), \tag{55}$$

where $\mathbf{S}$ consists of a purely volumetric elastic contribution $\mathbf{S}_{\text{vol}}$, a purely isochoric elastic contribution $\mathbf{S}_{\text{iso}}$ and additional internal tensor variables $\mathbf{Q}_\upsilon$, $\upsilon = 1, \ldots, m$, which may be interpreted as non-equilibrium stresses in the sense of non-equilibrium thermodynamics that are related to $\boldsymbol{\Gamma}_\upsilon$, $\upsilon = 1, \ldots, m$, [27].

The volumetric stress contribution is defined as

$$\mathbf{S}_{\text{vol}} = Jp^\star\mathbf{C}^{-1}, \qquad p^\star = \frac{\mathrm{d}\Psi_{\text{vol}}(J)}{\mathrm{d}J}. \tag{56}$$

By means of the fourth-order Lagrangian projection tensor $\mathbb{P} = \mathbb{I} - (\mathbf{C}^{-1} \otimes \mathbf{C})/3$, where $\mathbb{I}$ is the symmetric part of the fourth-order identity tensor, we define the deviatoric (isochoric) part of the second Piola–Kirchhoff stress tensor as [27]

$$\mathbf{S}_{\text{iso}} = J^{-2/3}\mathbb{P} : \widetilde{\mathbf{S}}, \tag{57}$$

where $\widetilde{\mathbf{S}} = 2\partial\Psi_{\text{iso}}/\partial\overline{\mathbf{C}}$ is referred to as the fictitious second Piola–Kirchhoff stress tensor. Hence, with (52) and a similar property to that in (10), a straightforward calculation gives

$$\widetilde{\mathbf{S}} = n\int_\Omega \rho(\mathbf{M})\bar{\lambda}^{-1}w'_{\text{iso}}(\bar{\lambda})\mathbf{M}\otimes\mathbf{M}\,\mathrm{d}\Omega + 2(1-\varphi)\frac{\partial\Psi_{\text{iso}}^{\text{mat}}(\overline{\mathbf{C}})}{\partial\overline{\mathbf{C}}}, \tag{58}$$

where the second term is the contribution of the isotropic matrix material. Here, and subsequently in this section, a prime indicates a derivative with respect to $\bar{\lambda}$.

The transient behavior is introduced through $\mathbf{Q}_\upsilon$ in (55), which is assumed to satisfy the evolution equations with the relaxation times τ_υ and the free-energy parameters θ_υ as material parameters, i.e.

$$\dot{\mathbf{Q}}_\upsilon + \frac{\mathbf{Q}_\upsilon}{\tau_\upsilon} = \theta_\upsilon \dot{\mathbf{S}}_{\text{iso}}, \tag{59}$$

where the dot denotes the material time derivative. The initial conditions at time $t = 0^+$ are assumed to be $\mathbf{Q}_\upsilon|_{t=0^+} = \mathbf{0}$. The present approach is characterized by two features which make it easy to apply to any existing hyperelastic constitutive model. First, the additive split of the free-energy function (54) allows one to evaluate both the elastic and the viscous contributions. Second, the algorithmic treatment of the transient equations discussed in [29, 30] results in a procedure to evaluate the time integrals which arise from (59). As far as the time scale for which the proposed model is applicable is concerned, it should be small enough so that linker binding/unbinding dynamics play a subordinate role and large enough so that viscous effects are small.

It should be mentioned here that a very different approach for examining the viscoelastic properties of cross-linked actin networks based on Brownian dynamics has been presented in [17]. It uses linear elasticity and viscoelasticity concepts with shear strains up to 0.55 without modeling the matrix in which the actin network is embedded. This approach is inappropriate for large deformations and finite element implementation. In contrast the continuum approach is fully nonlinear and easily implemented within a finite element framework.

3.2 Cauchy Stress Tensor

The Cauchy stress tensor $\boldsymbol{\sigma}$ is obtained by the push-forward $\boldsymbol{\sigma} = J^{-1}\mathbf{F}\mathbf{S}\mathbf{F}^{\mathrm{T}}$ of (55). Hence, we obtain the additive decomposition

$$\boldsymbol{\sigma} = \boldsymbol{\sigma}_{\mathrm{vol}} + \boldsymbol{\sigma}_{\mathrm{iso}} + \sum_{\upsilon=1}^{m} \mathbf{q}_{\upsilon}, \tag{60}$$

where $\boldsymbol{\sigma}_{\mathrm{vol}} = p^{\star}(J)\mathbf{I}$ is the purely volumetric stress contribution, with $p^{\star}$ defined in $(56)_2$. The fourth-order Eulerian projection tensor $\mathbb{P} = \mathbb{I} - (\mathbf{I} \otimes \mathbf{I})/3$ is used to obtain the isochoric (deviatoric) part $\boldsymbol{\sigma}_{\mathrm{iso}}$ of the Cauchy stress tensor, i.e.

$$\boldsymbol{\sigma}_{\mathrm{iso}} = \mathbb{P} : \widetilde{\boldsymbol{\sigma}}, \tag{61}$$

where $\widetilde{\boldsymbol{\sigma}} = J^{-1}\overline{\mathbf{F}}\tilde{\mathbf{S}}\overline{\mathbf{F}}^{\mathrm{T}}$ is the fictitious Cauchy stress tensor. With $\overline{\mathbf{m}}$ defined by (50) this can then be evaluated as

$$\widetilde{\boldsymbol{\sigma}} = nJ^{-1} \int_{\Omega} \rho(\mathbf{M})\bar{\lambda}^{-1} w'_{\mathrm{iso}}(\bar{\lambda})\overline{\mathbf{m}} \otimes \overline{\mathbf{m}}\, \mathrm{d}\Omega + 2(1-\varphi)J^{-1}\overline{\mathbf{F}}\frac{\partial \Psi^{\mathrm{mat}}_{\mathrm{iso}}}{\partial \overline{\mathbf{C}}}\overline{\mathbf{F}}^{\mathrm{T}}. \tag{62}$$

The spatial form of $\mathbf{Q}_{\upsilon}$, as used in (60), is simply given by $\mathbf{q}_{\upsilon} = J^{-1}\mathbf{F}\mathbf{Q}_{\upsilon}\mathbf{F}^{\mathrm{T}}$.

3.3 Elasticity Tensor

The linearization of the weak form of the equilibrium equations in finite element programs requires an appropriate elasticity tensor, and here we use the Eulerian elasticity tensor, denoted $\mathbb{c}$, and the related Cauchy stress tensor $\boldsymbol{\sigma}$. The structure of the free-energy function Ψ in terms of the additive decomposition carries over to the so-called algorithmic elasticity tensor. Hence, at a certain time the Eulerian form of the elasticity tensor may be written in the form

$$\mathbb{c} = \mathbb{c}_{\mathrm{vol}} + \mathbb{c}_{\mathrm{iso}} + \sum_{\upsilon=1}^{m} \mathbb{c}_{\mathrm{vis}\,\upsilon}. \tag{63}$$

In this relation $\mathbb{c}_{\text{vol}} = \tilde{p}\mathbf{I}\otimes\mathbf{I} - 2p^{\star}\mathbb{I}$, with $\tilde{p} = p^{\star} + J\mathrm{d}p^{\star}/\mathrm{d}J$, is the purely volumetric contribution. The purely isochoric contribution is [31]

$$\mathbb{C}_{\text{iso}} = \mathbb{P} : \widetilde{\mathbb{C}} : \mathbb{P} + \frac{2}{3}\mathrm{tr}(\widetilde{\boldsymbol{\sigma}})\mathbb{P} - \frac{2}{3}(\boldsymbol{\sigma}_{\text{iso}}\otimes\mathbf{I} + \mathbf{I}\otimes\boldsymbol{\sigma}_{\text{iso}}), \tag{64}$$

with the definition of the fourth-order fictitious elasticity tensor $\widetilde{\mathbb{c}}$ in the spatial description, which, in index notation, is given by $(\widetilde{\mathbb{c}})_{abcd} = 4J^{-1}\overline{F}_{aA}\overline{F}_{bB}\overline{F}_{cC}\overline{F}_{dD}\,[\partial^2\Psi_{\text{iso}}(\overline{\mathbf{C}})/\partial\overline{\mathbf{C}}\partial\overline{\mathbf{C}}]_{ABCD}$, where $\overline{F}_{iI}$ are components of the isochoric deformation gradient (see [14, Appendix] for details). With the help of (58) it is straightforward to obtain

$$\begin{aligned} 4\frac{\partial^2\Psi_{\text{iso}}(\overline{\mathbf{C}})}{\partial\overline{\mathbf{C}}\partial\overline{\mathbf{C}}} = n\int_{\Omega}\rho(\mathbf{M})\bar{\lambda}^{-2}[w''_{\text{iso}}(\bar{\lambda}) - \bar{\lambda}^{-1}w'_{\text{iso}}(\bar{\lambda})]\mathbf{M}\otimes\mathbf{M}\otimes\mathbf{M}\otimes\mathbf{M}\,\mathrm{d}\Omega \\ +4(1-\varphi)\frac{\partial^2\Psi^{\text{mat}}_{\text{iso}}(\overline{\mathbf{C}})}{\partial\overline{\mathbf{C}}\partial\overline{\mathbf{C}}}, \end{aligned} \tag{65}$$

where the shorthand notation $(\bullet)'' = \mathrm{d}(\bullet)'/\mathrm{d}\bar{\lambda}$ has been used. Finally, with the use of (50) we obtain the fictitious elasticity tensor

$$\widetilde{\mathbb{C}} = nJ^{-1}\int_{\Omega}\rho(\mathbf{M})[w''_{\text{iso}}(\bar{\lambda}) - \bar{\lambda}^{-1}w'_{\text{iso}}(\bar{\lambda})]\bar{\lambda}^{-2}\overline{\mathbf{m}}\otimes\overline{\mathbf{m}}\otimes\overline{\mathbf{m}}\otimes\overline{\mathbf{m}}\,\mathrm{d}\Omega + \widetilde{\mathbb{C}}^{\text{mat}}_{\text{iso}}, \tag{66}$$

where the index notation of the tensor $\widetilde{\mathbb{C}}^{\text{mat}}_{\text{iso}}$ is given by $(\widetilde{\mathbb{C}}^{\text{mat}}_{\text{iso}})_{abcd} = 4J^{-1}(1-\varphi)\overline{F}_{aA}\overline{F}_{bB}\overline{F}_{cC}\overline{F}_{dD}$ $[\partial^2\Psi^{\text{mat}}_{\text{iso}}(\overline{\mathbf{C}})/\partial\overline{\mathbf{C}}\partial\overline{\mathbf{C}}]_{ABCD}$. For the explicit expression of the algorithmic tensor $\mathbb{c}_{\text{vis}\,v}$, the viscous contribution in the Eulerian description, the reader is referred to [20, 32].

It is worth emphasizing that different filament models are easily incorporated into a nonlinear finite element scheme by simply changing the function w_{iso}, and therefore w'_{iso} and w''_{iso}, in (58) and (66).

4 Numerical Treatment and Representative Example

In the considerations in Section 2, we employed an inextensible filament model. The asymptotes arising from this formulation, however, may cause unfavorable conditions within a numerical solution procedure such as the finite element method. In order to increase the reliability of the Newton–Raphson algorithm, we subsequently use the extensible version of the filament model introduced in Appendix A. The extensibility of the filament is modulated by the additional material parameter μ_0, the stretch modulus. This version of the model has proved to be suitable for fitting data from stretching experiments conducted on single actin filaments in the high as well as in the low stretch regime [14].

The integrals over the unit sphere such as those in (58), (62), (66) or (9) are evaluated using standard numerical procedures, e.g., the adaptive Simpson quadrature, as implemented in `MATLAB` (MathWorks, Inc., Natick, MA, USA). However, this method is very costly in terms of computation and is only viable for basic analyses, such as those described in the previous sections. For solving more complex problems we need a more efficient scheme. An excellent method for the evaluation of integrals over a sphere was suggested by Bažant and Oh [33] with $m = 42$ distinct direction vectors $\mathbf{M}^i$, $i = 1, 2, \ldots, m$. The integrals transform then according to

$$\int_\Omega \mathbf{A}(\mathbf{M})\, \mathrm{d}\Omega \sim 4\pi \sum_{i=1}^{n} \mathbf{A}(\mathbf{M}^i) q^i, \tag{67}$$

where $\mathbf{A}$ is a tensor-valued function and q^i are the integration weights. A table with the direction vectors and the associated integration weights can be found in [33, Table 1]. The symmetry of the method together with the symmetry discussed in Section 2.2 allows us to use only half of the directions and double the integration weights.

We have implemented the proposed model according to the formulation in Section 3 in the open source finite element analysis program FEAP [34]. In order to avoid volumetric locking, we use a finite element which is based on a three-field variational principle.

4.1 Application to Micropipette Aspiration

The proposed model should be calibrated with data obtained from rheometer experiments before it is used to interpret the outcome of experiments with more complicated geometry and boundary conditions. Indentation by atomic force microscopy and micropipette aspiration are two examples of techniques that are used to determine the mechanical properties of cell constituents and of whole cells. In the following, we concentrate on the latter and consider the impact of different linkers and viscosities.

The setup of the virtual experiment is similar to that described in [30] and inspired by *in vitro* experiments on cells (see, e.g., [35, 36]). As considered in [37] the droplet consisting of a cross-linked actin envelope and a very soft inside is aspirated into a micropipette, as depicted in Fig. 7(a), which shows half of the axisymmetric structure. The inside of the droplet is only required to achieve numerical stability during the calculations and its contribution to the overall mechanical response is negligible because it is assumed to be much less stiff than the envelope material. The droplet has a radius of $r_{\mathrm{d}} = 7\,\mu\mathrm{m}$ and the actin envelope is $1\,\mu\mathrm{m}$ thick; the bold blue semicircle in Fig. 7(a) denotes the interface. The micropipette has a radius $r_{\mathrm{p}} = 5\,\mu\mathrm{m}$ and its end is rounded with a radius of $r_{\mathrm{m}} = 0.75\,\mu\mathrm{m}$. The pressure difference between the environment and the micropipette is achieved by applying a suction pressure p_{i} (i.e. a tensile follower load) on those nodes of the axisymmetric setup which lie inside the micropipette.

Between the rigid micropipette and the surface of the droplet, we employ a frictionless contact condition.

The constitutive relation for the actin envelope is taken to be the model considered in Appendix A, i.e. an isotropic cross-linked network of extensible filaments with the compliant linkers discussed in Section 2.5. The viscoelasticity of the material is considered by taking one internal variable in (54) into account. We use the material parameters from the Sections 2.4 and 2.5, specifically the end-to-end distance $r_{0,\mathrm{f}} = 1.63\,\mu\mathrm{m}$ at zero force of the filament, the contour length $L = 1.96\,\mu\mathrm{m}$, the persistence length $L_{\mathrm{p}} = 16\,\mu\mathrm{m}$, the filament density $n = 7.66\,\mu\mathrm{m}^{-3}$, the temperature $T = 294\,\mathrm{K}$ and $\delta = 2$. We choose a very small end-to-end distance $r_{0,\mathrm{c}}$, which, for definiteness, we set at $r_{0,\mathrm{c}} = 14\,\mathrm{nm}$ [38, p. 1007], since we have found that different choices in the nanometer range do not effect the results significantly. The extensibility of the filaments is characterized by the stretch modulus $\mu_0 = 38.6\,\mathrm{nN}$ [14]. The parameter values for the viscous part, the free-energy parameter $\theta = 0.835$ and the relaxation time $\tau = 2\,\mathrm{s}$, are adopted from [14]. The penalty method used to achieve incompressibility requires the penalty parameter κ; see $(53)_1$. In preliminary studies we used values for κ which were large enough to ensure incompressibility (the results of the computations converged as κ was increased) and small enough to allow stable computations, specifically in the range of 1–10 kPa. The soft inside material is taken to be a compressible neo-Hookean model of the form

$$\Psi = \left(\kappa - \frac{2}{3}\mu\right)\mathcal{G}(J) + \frac{\mu}{2}(I_1 - 2\ln J - 3), \tag{68}$$

where the function $\mathcal{G}$ is given in $(53)_2$. The parameter κ, which is now the bulk modulus in the reference configuration, and the shear modulus μ relate to the Young's modulus E and the

Poisson's ratio ν according to

$$\kappa = \frac{E}{3(1-2\nu)}, \qquad \mu = \frac{E}{2(1+\nu)}. \tag{69}$$

For the simulation the Young's modulus E was taken to be $10\,\mathrm{Pa}$, which is $1/10$ of that of the envelope material, while ν was taken to be 0.4.

In a first simulation the micropipette fully aspirates the droplet very slowly, i.e. in a quasi-static manner, for relative linker stiffnesses $\eta = 1,\, 2/3,\, 1/3$. In Fig. 7(b), the aspiration length L_a is plotted as a function of the pressure difference Δp between the environment (here with pressure zero) and the inside of the micropipette (p_i), i.e. $\Delta p = p_\mathrm{i}$. Note that for a droplet, L_a is larger than zero in the reference configuration because of its curvature. In our example, the value of L_a at the start of the experiment is $2\,\mu\mathrm{m}$. The numerical results shown in Fig. 7(b) are characterized by a linear part at low pressure differences, as was observed experimentally [35, 36]. The linear part is followed by a rapidly increasing slope for which a small increase in pressure causes a large increase in aspiration length and when the droplet is almost fully aspirated the tangent to the curves becomes vertical, indicating a possible instability. This has implications for the numerical solution because the deformation in one time step becomes large and eventually the Newton–Raphson algorithm fails. This happens at decreasing pressures for decreasing values of η. This means that the lower the stiffness of the droplet the smaller is the pressure difference required to fully aspirate it. Higher aspiration lengths are produced at a specified pressure difference for network materials with lower stiffnesses.

The second simulation shows the influence of the viscosity of the material on the aspiration response. The droplet is aspirated only partly and then allowed to creep further inside the micropipette. The pressure difference is increased to $4\,\mathrm{Pa}$ within $2\,\mathrm{s}$ and then held constant for

another $38\,\mathrm{s}$, beyond which there were no significant changes and the simulation was stopped. Figure 7(c) shows the aspiration length L_a versus time t. The linker stiffness is fixed at $\eta = 2/3$, while three different values of τ are used (4, 2 and $1\,\mathrm{s}$). The paths of the curves for all relaxation times resemble typical creep behavior in aspiration tests on cells [35, 36]. At the time $t = 2\,\mathrm{s}$ after which the pressure is constant the aspiration length is about $L_\mathrm{a} = 4.2\,\mu\mathrm{m}$ in each case. Thereafter, the droplets creep further inside the micropipette at different rates, depending on the relaxation time τ. Specifically, for a shorter relaxation time the droplet creeps faster. For each relaxation time the aspiration length approaches a steady state value of about $4.7\,\mu\mathrm{m}$.

5 Summary and Concluding Remarks

In the present work we have proposed a general incompressible affine network model for which filaments are distributed arbitrarily within an isotropic matrix. We have derived the associated Cauchy stress tensor and applied it to a simple shear deformation. The contributions of the filaments correctly reproduce the normal stress response of isotropically cross-linked actin networks obtained from rheological experiments [2]. By using scaling arguments to estimate the material parameters we have obtained a stress–strain behavior comparable to that determined from experimental results from actin–HMM networks. By using the same actin protein concentrations as for actin–HMM networks, stiffnesses can be lowered by using compliant linkers, thus reflecting the softer response of actin–filamin networks. Within a finite element framework incompressibility is enforced by using a penalty function in a compressible formulation of the model and an expression for the elasticity tensor is provided. Viscoelastic effects are also included in an additive way. Finite element calculations simulating micropipette aspiration have

produced results similar to those obtained from cell experiments.

Continuum mechanics provides a very powerful framework within which to analyze the multi-scale features of networks. It forms a basis for the solution of complex boundary-value problems, based on finite element implementation, which are highly relevant to biomechanical applications, in particular for solving problems of biomedical interest. We have provided both the analytical and finite element regimes for applications of the model. The model can include various levels of refinement such as the basic inclusion of cross-linking that we have discussed here, or more sophisticated versions of the cross-linking contribution which will form the basis of future work. A new feature is that we have illustrated the mechanical influence of the linker stiffness on the overall mechanical behavior, and the model has also being able for the first time analytically to predict the negative normal stress effect in simple shear. The finite element implementation of the new model has produced a new elasticity tensor which is an important input for computational biomechanics. It is also straightforward to include viscoelastic effects, which are crucial for the analysis of F-actin networks.

Within the present study we have employed a number of assumptions that may lead to limitations of the model. We now briefly review these assumptions and discuss their justifications. The incompressible network model introduced in Section 2 and its extension in Section 3 is based on five basic simplifications concerning the filaments: (i) they deform in an affine manner; (ii) they have equal lengths between linker proteins (iii) they have equal material properties; (iv) they can only support tensile loads and are ineffective under compression; (v) there is no mechanical coupling between any filaments connected through a linker.

The first assumption is justified for densely cross-linked networks [5], i.e. relatively high

actin and linker concentrations, which is the focus of our analysis. The second and third assumptions are acceptable if the number of filaments involved in an experiment is large enough so that we may use their average behavior (homogenization). We are confident that these three assumptions are legitimate because of the sizes of the volumes of the samples used in bulk rheology. Since actin filaments are very thin compared with their lengths, compressive forces will be barely noticeable, and thus the fourth assumption is justified. The last assumption has been adopted because little is known about the interaction between two individual filaments connected by a linker.

In Sections 2 and 3 we have used the additional simplification of isotropy although the proposed model does not require this in general. Reconstituted actin networks have been shown to possess isotropy [7]. Cells, however, are not in general isotropic. Future work should include the determination of the anisotropic structure of living cells in terms of, for example, the angular density $\rho(\mathbf{M})$. The inextensible filament model limits the analysis to moderate levels of shear strain, but the associated locking of the model may be overcome by using an extensible model, as in the numerical example in Section 4. The analytical considerations in Section 2 have been conducted for purely elastic materials including the effect of linkers that support axial loads. However, cross-linked actin networks clearly exhibit viscous properties and these can be taken into account by including viscous contributions such as those described in Section 3.

In conclusion, we are easily able to perform numerical studies in which only one parameter at a time is varied. In particular, different filament models are easily incorporated into a nonlinear finite element program by changing the filament free-energy function w_{iso}. Hence, the influence of phenomena known in cell mechanics may be studied in more detail using this

model, and therefore may indicate the type of experimental data that would be useful for interpreting the results theoretically.

Appendix A

The inextensible filament model (36) is given in dimensionless form as

$$f^\star(\lambda) = f\frac{L^2}{\pi^2 B_0} = \left(\frac{a-1}{a-\lambda}\right)^\delta - 1. \tag{70}$$

We now extend it to the extensible case by following the references [14, 21, 22]. We introduce the stretch modulus μ_0, and define the shorthand notation $\alpha = \pi^2 B_0/(\mu_0 L^2)$. Then the required relationship is given in inverse and dimensionless form as

$$\lambda = a(1+\alpha f^\star) - \frac{(1+2\alpha f^\star)(1+\alpha f^\star)^{1/\delta}}{(1+f^\star+\alpha f^{\star 2})^{1/\delta}}(a-1). \tag{71}$$

Defining the dimensionless free energy as

$$w^\star(\lambda) = \frac{L^2}{\pi^2 r_0 B_0} w(\lambda) \tag{72}$$

we obtain the first and second derivatives of $w^\star(\lambda)$ with respect to λ as

$$w^{\star\prime} = f^\star, \tag{73}$$

$$w^{\star\prime\prime} = \frac{1}{\alpha a\delta + \left(\dfrac{(1+2\alpha f^\star)^2}{1+f^\star+\alpha f^{\star 2}} - \alpha\dfrac{1+2\alpha f^\star}{1+\alpha f^\star} - 2\alpha\delta\right)\left(\dfrac{1+\alpha f^\star}{1+f^\star+\alpha f^{\star 2}}\right)^{1/\delta}(a-1)}. \tag{74}$$

Both the first and second derivatives are required in a finite element implementation. By taking $\alpha \to 0$ we obtain, for the inextensible case,

$$w^{\star\prime\prime} = \frac{\delta(1+f^\star)^{\frac{\delta+1}{\delta}}}{a-1}. \tag{75}$$

In [21], where the notation $\beta + 1$ was used instead of δ, and it was shown for the inextensible case that for $\delta = 1$ and $\delta = 2$ the following expressions hold

$$\frac{r_0}{L} = 1 - \frac{L}{\pi^2 L_p}, \qquad \frac{r_0}{L} = 1 - \frac{L}{\pi^{3/2} L_p}, \tag{76}$$

respectively, where L_p is the persistence length. For a general δ this can be generalized to

$$\frac{r_0}{L} = 1 - \frac{L}{\pi^{\frac{1+\delta}{\delta}} L_p}. \tag{77}$$

References

[1] P. A. Janmey, S. Hvidt, J. Lamb, and T. P. Stossel. Resemblance of actin-binding protein/actin gels to covalently crosslinked networks. *Nature*, 345:89–92, 1990.

[2] P. A. Janmey, M. E. McCormick, S. Rammensee, J. L. Leight, P. C. Georges, and F. C. MacKintosh. Negative normal stress in semiflexible polymer gels. *Nat. Mater.*, 6:48–51, 2007.

[3] M. L. Gardel, F. Nakamura, J. H. Hartwig, J. C. Crocker, T. P. Stossel, and D. A. Weitz. Prestressed F–actin networks cross–linked by hinged filamins replicate mechanical properties of cells. *PNAS*, 103:1762–1767, 2006.

[4] K. M. Schmoller, O. Lieleg, and A. R. Bausch. Cross-linking molecules modify composite actin networks independently. *Phys. Rev. Lett.*, 101:118102, 2008.

[5] M. L. Gardel, J. H. Shin, F. C. MacKintosh, L. Mahadevan, P. Matsudaira, and D. A. Weitz. Elastic behavior of cross-linked and bundled actin networks. *Science*, 304:1301–1305, 2004.

[6] J. H. Shin, M. L. Gardel, L. Mahadevan, P. Matsudaira, and D. A. Weitz. Relating microstructure to rheology of a bundled and cross-linked F-actin network in vitro. *PNAS*, 101:9636–9641, 2004.

[7] R. Tharmann, M. M. Claessens, and A. R. Bausch. Viscoelasticity of isotropically cross–linked actin networks. *Phys. Rev. Lett.*, 98:088103, 2007.

[8] O. Lieleg, M. M. A. E. Claessens, Y. Luan, and A. R. Bausch. Transient binding and dissipation in semi-flexible polymer networks. *Phys. Rev. Lett.*, 101:108101, 2008.

[9] Y. Lanir. Constitutive equations for fibrous connective tissues. *J. Biomech.*, 16:1–12, 1983.

[10] C. Miehe, S. Göktepe, and F. Lulei. A micro-macro approach to rubber-like materials – Part I: The non-affine micro-sphere model of rubber elasticity. *J. Mech. Phys. Solids*, 52: 2617–2660, 2004.

[11] V. Alastrué, M. A. Martinez, M. Doblaré, and A. Menzel. Anisotropic micro–sphere–based finite elasticity applied to blood vessel modelling. *J. Mech. Phys. Solids*, 57:178–203, 2009.

[12] S. Federico and T. C. Gasser. Nonlinear elasticity of biological tissues with statistical fibre orientation. *J. R. Soc. Interface*, 7:955–966, 2010.

[13] J. S. Palmer and M. C. Boyce. Constitutive modeling of the stress-strain behavior of F-actin filament networks. *Acta Biomater.*, 4:597–612, 2008.

[14] M. J. Unterberger, K. M. Schmoller, A. R. Bausch, and G. A. Holzapfel. A new approach

to model cross-linked actin networks: Multi-scale continuum formulation and computational analysis. *J. Mech. Behav. Biomed. Mater.*, 22:95–114, 2013.

[15] M. Tkachuk and C. Linder. The maximal advance path constraint for the homogenization of materials with random network microstructure. *Philos. Mag.*, 92:2779–2808, 2012.

[16] Q. Wen and P. A. Janmey. Polymer physics of the cytoskeleton. *Curr. Opin. Solid State Mater. Sci.*, 15:177–182, 2011.

[17] T. Kim, W. Hwang, H. Lee, and R. D. Kamm. Computational analysis of viscoelastic properties of crosslinked actin networks. *PLoS Comput. Biol.*, 5:e1000439, 2009.

[18] C. Storm, J. J. Pastore, F. C. MacKintosh, T. C. Lubensky, and P. A. Janmey. Nonlinear elasticity in biological gels. *Nature*, 435:191–194, 2005.

[19] R. W. Ogden. *Non-linear Elastic Deformations*. Dover, New York, 1997.

[20] G. A. Holzapfel. *Nonlinear Solid Mechanics. A Continuum Approach for Engineering*. John Wiley & Sons, Chichester, 2000.

[21] G. A. Holzapfel and R. W. Ogden. Elasticity of biopolymer filaments. *Acta Biomater.*, 9: 7320–7325, 2013.

[22] G. A. Holzapfel and R. W. Ogden. On the bending and stretching elasticity of biopolymer filaments. *J. Elasticity*, 104:319–342, 2011.

[23] F. C. MacKintosh, J. Käs, and P. A. Janmey. Elasticity of semiflexible biopolymer networks. *Phys. Rev. Lett.*, 75:4425–4428, 1995.

[24] L. Le Goff, O. Hallatschek, E. Frey, and F. Amblard. Tracer studies on F-actin fluctuations. *Phys. Rev. Lett.*, 89:258101, 2002.

[25] K. M. Schmoller, O. Lieleg, and A. R. Bausch. Structural and viscoelastic properties of actin/filamin networks: Cross-linked versus bundled networks. *Biophys. J.*, 97:83–89, 2009.

[26] P. Chen. Anomalous normal stresses in biopolymer networks with compliant cross-links. *EPL (Europhysics Letters)*, 105:38003-p1, 2014.

[27] G. A. Holzapfel, T. C. Gasser, and R. W. Ogden. A new constitutive framework for arterial wall mechanics and a comparative study of material models. *J. Elasticity*, 61:1–48, 2000.

[28] J. C. Simo. On a fully three-dimensional finite-strain viscoelastic damage model: Formulation and computational aspects. *Comput. Meth. Appl. Mech. Eng.*, 60:153–173, 1987.

[29] G. A. Holzapfel. On large strain viscoelasticity: Continuum formulation and finite element applications to elastomeric structures. *Int. J. Numer. Meth. Engng*, 39:3903–3926, 1996.

[30] M. J. Unterberger, K. M. Schmoller, C. Wurm, A. R. Bausch, and G. A. Holzapfel. Viscoelasticity of cross-linked actin networks: experimental tests, mechanical modeling and finite element analysis. *Acta Biomater.*, 9:7343–7353, 2013.

[31] C. Miehe. Aspects of the formulation and finite element implementation of large strain isotropic elasticity. *Int. J. Numer. Meth. Engng*, 37:1981–2004, 1994.

[32] G. A. Holzapfel and T. C. Gasser. A viscoelastic model for fiber-reinforced composites at

finite strains: Continuum basis, computational aspects and applications. *Comput. Meth. Appl. Mech. Eng.*, 190:4379–4403, 2001.

[33] Z. P. Bažant and B. H. Oh. Efficient numerical integration on the surface of a sphere. *Z. Angew. Math. Mech.*, 66:37–49, 1986.

[34] *FEAP – A Finite Element Analysis Program, Version 8.2 User Manual*. University of California at Berkeley, Berkeley, California, 2008.

[35] W. R. Jones, H. P. Ting-Beall, G. M. Lee, S. S. Kelley, R. M. Hochmuth, and F. Guilak. Alterations in the Young's modulus and volumetric properties of chondrocytes isolated from normal and osteoarthritic human cartilage. *J. Biomech.*, 32:119–127, 1999.

[36] E. Zhou, S. Quek, and C. Lim. Power-law rheology analysis of cells undergoing micropipette aspiration. *Biomech. Model. Mechanobiol.*, 9:563–572, 2010.

[37] E. Monteiro, J. Yvonnet, Q.-C. He, O. Cardoso, and A. Asnacios. Analyzing the interplay between single cell rheology and force generation through large deformation finite element models. *Biomech. Model. Mechanobiol.*, 10:813–830, 2011.

[38] B. Alberts, A. Johnson, J. Lewis, M. Raff, K. Roberts, and P. Walter. *Molecular Biology of the Cell*. Garland Science, New York, 5th edition, 2008.

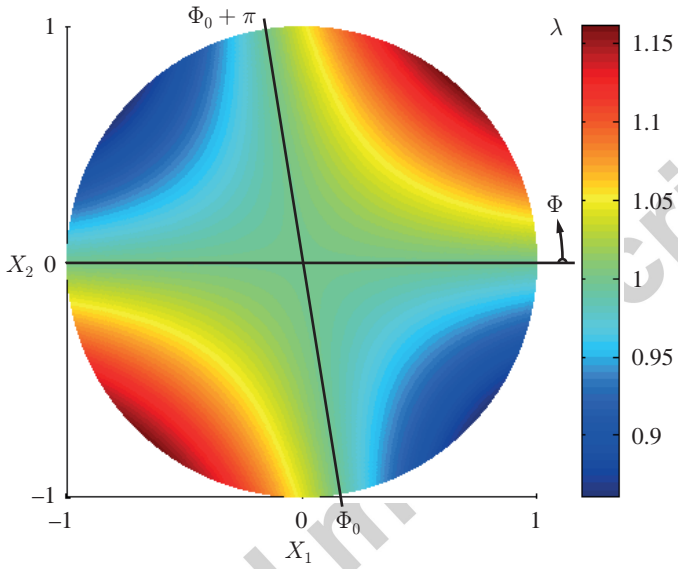

Figure 1: The value of the stretch λ given by (14) plotted in the (X_1,X_2)-plane for $\gamma = 0.3$, where $X_1 = \sin\Theta\cos\Phi$, $X_2 = \sin\Theta\sin\Phi$. The horizontal black line corresponds to $\Phi = 0$ and $\lambda = 1$, while the sloping line also corresponds to $\lambda = 1$ but with $\Phi = \Phi_0$ or $\Phi = \Phi_0 + \pi$. The plot is qualitatively the same for all values of Θ except for $\Theta = 0$, in which case $\lambda = 1$.

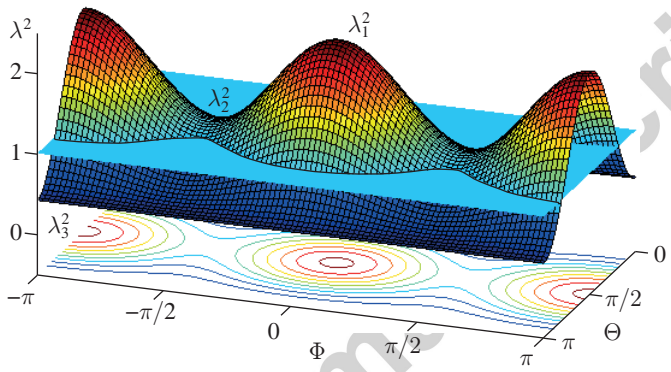

Figure 2: Squared stretch λ^2 plotted as a function of the spherical angles Θ and Φ, where $\lambda_1 > \lambda_2 > 1$ and λ_3 are the principal stretches. The relevant integration domain lies above the plane defined by $\lambda^2 = 1$.

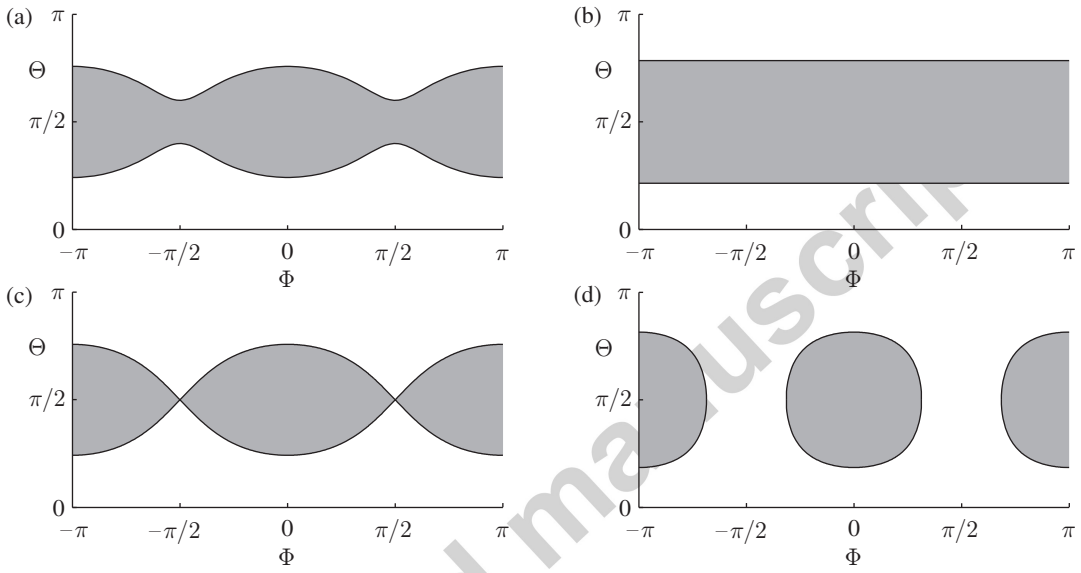

Figure 3: The grey shaded areas are the integration domains for different deformation types: (a) $\lambda_1 > \lambda_2 > 1$ with the particular values from Fig. 2; (b) equibiaxial extension or unconfined compression ($\lambda_1 = \lambda_2 > 1$); (c) pure shear or simple shear in the (1,3)-plane ($\lambda_1 > 1 = \lambda_2$); (d) uniaxial extension ($\lambda_1 > 1$ with $\lambda_2 = \lambda_3$).

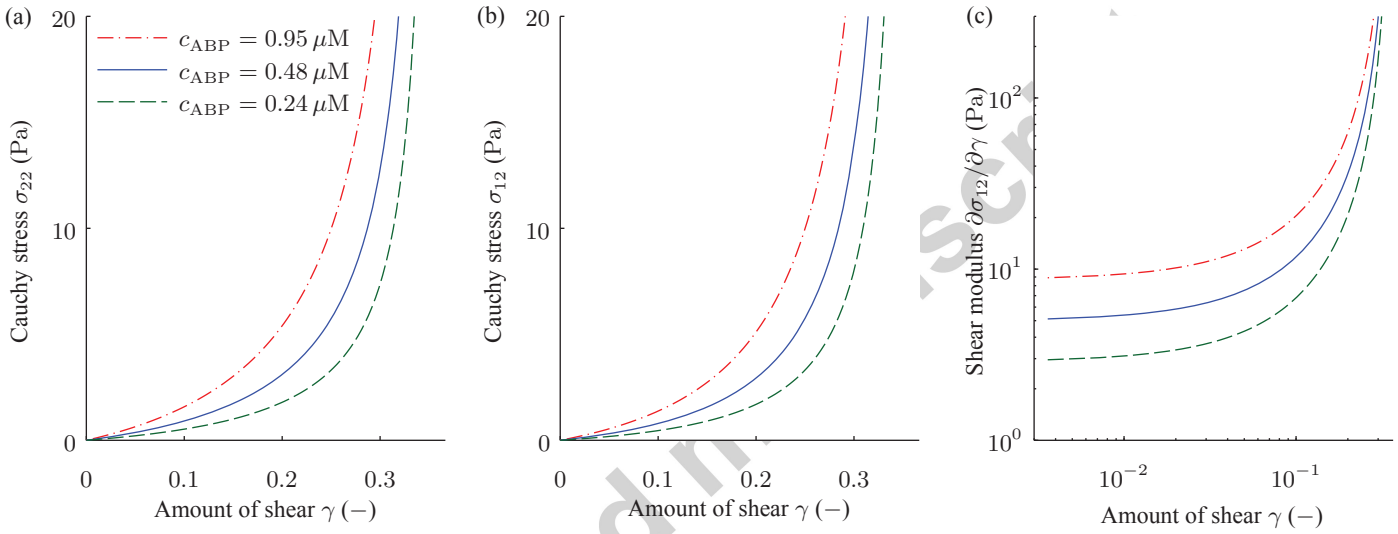

Figure 4: Predictions of the model for simple shear with varying concentrations of actin-binding proteins, $c_{\mathrm{ABP}} = 0.95$, 0.475 and $0.238\,\mu\mathrm{M}$: (a) normal stress σ_{22}; (b) shear stress σ_{12}; (c) shear modulus $\partial\sigma_{12}/\partial\gamma$ versus amount of shear γ.

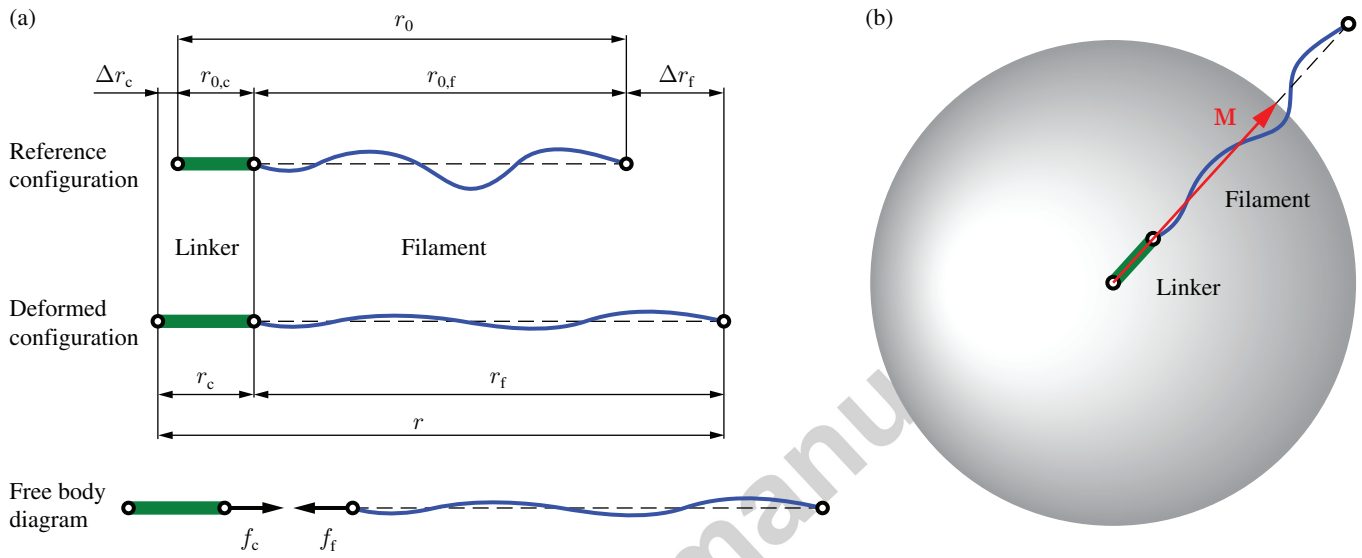

Figure 5: Filament with linker: (a) filament compound consisting of a filament (blue, wavy curve) and a linker (bold, green line) with end-to-end distances at zero force $r_{0,\mathrm{f}}$ and $r_{0,\mathrm{c}}$, respectively, and their total r_0. The deformed end-to-end distances are r_{f} and r_{c} with their total r. The elongation is divided into filament elongation Δr_{f} and linker elongation Δr_{c}. The free body diagram illustrates the equilibrium state $f_{\mathrm{f}} = f_{\mathrm{c}}$. (b) Filament compound in the reference configuration oriented in space within a micro-sphere in the direction $\mathbf{M}$.

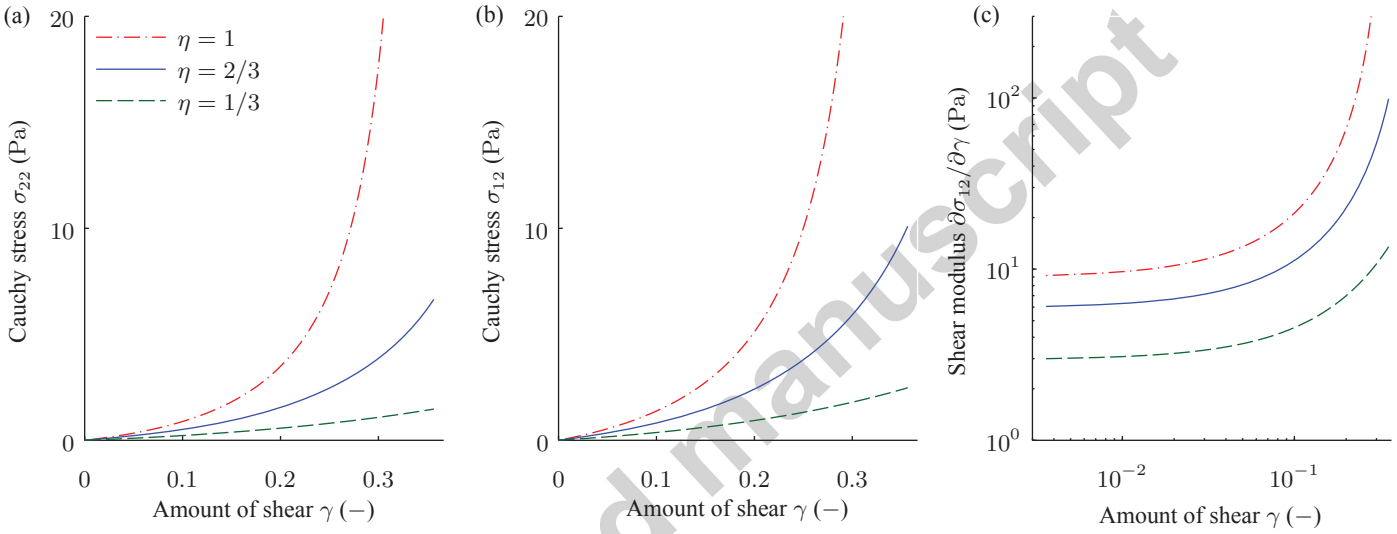

Figure 6: Predictions of the model for simple shear with constant concentrations of actin-binding proteins and relative linker stiffnesses $\eta = 1,\ 2/3,\ 1/3$: (a) normal stress σ_{22}; (b) shear stress σ_{12}; (c) shear modulus $\partial\sigma_{12}/\partial\gamma$ versus amount of shear γ.

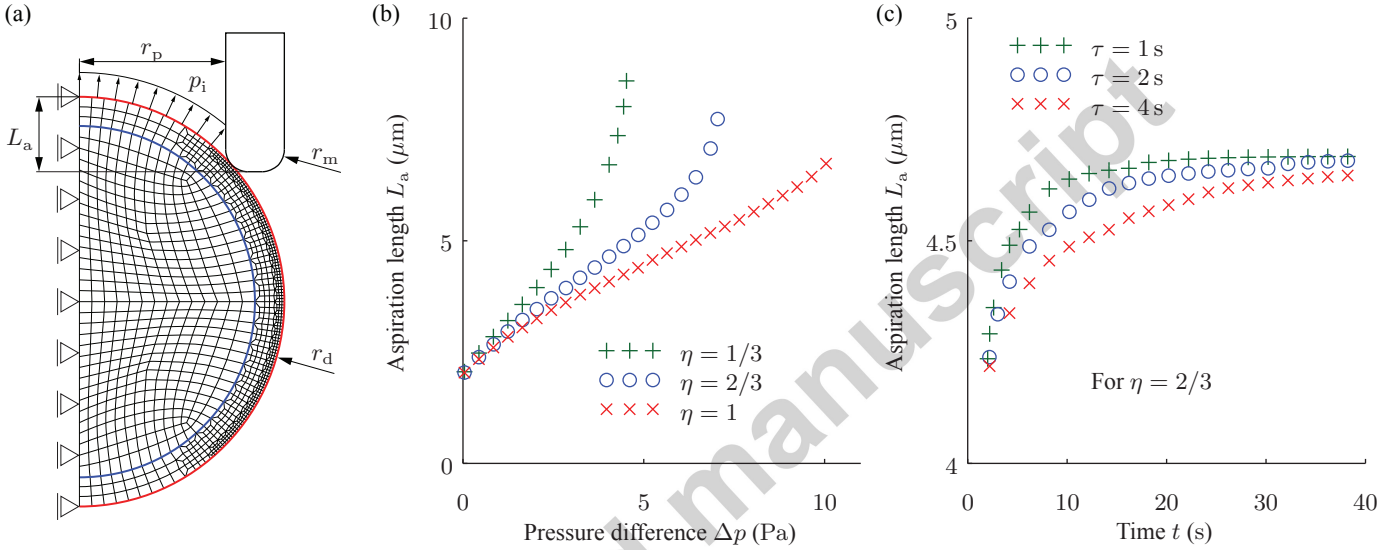

Figure 7: Micropipette aspiration of a droplet consisting of a cross-linked actin envelope and a very soft inside: (a) geometry and boundary conditions of half the axisymmetric structure; (b) aspiration length L_a versus pressure difference Δp for relative linker stiffnesses, $\eta = 1,\ 2/3,\ 1/3$; (c) aspiration length L_a versus time t for relaxation times, $\tau = 4,\ 2,\ 1\,\mathrm{s}$, for $\eta = 2/3$.